Human adipose stromal cells differentiate towards a tendon phenotype with extracellular matrix production and adapted visco-elastic properties in a 3D-culture system

Maxime Hordé, Jonathan Fouchard, Xavier Laffray, Cédrine Blavet, Véronique Bérézіat, Claire Lagathu, Ludovic Gaut, Delphine Duprez, Emmanuelle Havis

Human adipose stromal cells differentiate towards a tendon phenotype with extracellular matrix production and adapted visco-elastic properties in a 3D-culture system

Maxime Hordé[a], Jonathan Fouchard[a], Xavier Laffray[b], Cédrine Blavet[a], Véronique Béréziat[c], Claire Lagathu[c], Ludovic Gaut [a], Delphine Duprez[a,1,#] and Emmanuelle Havis[a,1,#]

[a] Sorbonne Université, Institut Biologie Paris Seine, CNRS UMR7622, Developmental Biology Laboratory, Inserm U1156, F-75005 Paris, France

[b] Université Paris Est Creteil, Glycobiology, Cell Growth and Tissue Repair Research Unit (Gly-CRRET), EA 4397, F-94010 Creteil, France.

[c]Sorbonne Université, Inserm UMRS938, Centre de Recherche Saint-Antoine (CRSA), Institut Hospitalo-Universitaire de Cardio-Métabolisme et Nutrition (ICAN), F-75012 Paris, France

[1] Co-senior authors; [#] Co-corresponding authors

Abstract

Tendons are composed of type I collagen fibrils and specialized extracellular matrix (ECM) proteins that are hierarchically organized to transmit forces from muscle to bone. Reliable and affordable models of human tendon constructs are requested to serve surgical treatment after tendon injury and in vitro pharmacological testing. Here, using human adipose stromal cells embedded in a 3D type-I collagen matrix and submitted to static uniaxial geometrical constraint, we generated human tendon constructs and assessed their mechanical properties and gene expression for up to 21 days in culture. The analysis of visco-elastic properties by nano-indentation indicated an increase in tissue stiffness (from about 1kPa at Day 0 to 10 kPa at Day 21), concomitant with a reduced percentage of stress relaxation, indicative of more solid-like mechanical properties. These changes in mechanical properties were associated with a reorganisation of ECM and the emergence of two cell populations, with one cell population organized as a ring in tissue periphery. In addition to the activation of the well-established tendon differentiation genetic program, assessed by the expression of *SCX*, *MKX*, *TNMD* and *COL1A1*, we validated the expression of a novel tendon marker, TM4SF1 and other components of the ECM such as *COL6A3*, *COL14A1*, *DPT*, *DCN*, *POSTN* and *THBS2*, which were previously identified in transcriptomic analyses of embryonic mouse limb tendons. In summary, this 3D culture system, which recapitulates most stages of tendon development, represent a potential route for human tendon regeneration.

Key words: tendon constructs, visco-elastic properties, extra cellular matrix, human adipose stromal cells

Introduction

The tendon is a connective tissue composed of a dense extracellular matrix (ECM) consisting mainly of type I collagen fibrils which are organised hierarchically to resist the tensile forces transmitted from the muscle to the bone and to allow locomotion. The incidence of ruptured tendons, particularly the Achilles tendon, has been rising steadily over the past decades [1,2] to reach the level of 37 per 100,000 population [3]. Compared to other components of the musculoskeletal system, little is known about the mechanisms involved in tendon development. This delay in knowledge slows the development of effective therapies for tendon repair, which remains a major clinical challenge in orthopaedic medicine [4].

Tendon constructs have been developed using human tendon fibroblasts [5] with similar mechanical properties to embryonic tendon tissue [6–8]. The aim of this study is to design and validate a model of human tendon development in a 3D-culture system from human stem cells, in order to eventually generate tendons in vitro from abundant and easy to obtain cells. Since the identification of pluripotent stem cells in the bone marrow stroma 55 years ago [9], the human Bone Marrow Mesenchymal Stromal Cells (hBM-MSC) have become a standard in the field of adult stem cell biology and in regenerative medicine, due to their high differentiation properties towards various cell lineages [10–13] including tendons [14–17]. Nevertheless, the bone marrow harvest is painful, with possible donor site morbidity, and the number of cells collected is usually low [18]. More recent publications and clinical trials have shown that adipose tissue can be considered an attractive alternative source of MSC, as it can be harvested by a minimally invasive procedure and can provide millions to billions of stem cells, called human Adipose-derived Stromal Cells (hASC) [19–22].

For many years, mesenchymal stromal cell differentiation into tendon cells has been demonstrated in traditional 2D-cell culture systems [23–27]. However, 2D-culture system is very different from the physiological context of tendon development and often fails to maintain the tendon phenotype over time [27,28]. The comparative analysis of 2D versus 3D MSC differentiation into tendons demonstrated that 3D-culture conditions are more favourable for tendon differentiation marker expression [29–32]. During embryonic development, tendon primordia are high-cell-density linear structures anchored between bone and muscle in formation. To mimic tendon embryonic development, 3D-culture systems consist in cells homogenously embedded in a matrix deposited between two anchor points and incubated within a bioreactor [33–35]. Most of the protocols are based on high density cell populations seeded in gels such as fibrin gels [23,27], collagen gels [33,36,37] or decellularized tendon scaffolds

[38]. In particular, human BM-MSCs cultured in 3D under uniaxial static tension exhibit a similar phenotype with embryonic progenitor tendon cells [15,16].

The transcription factors SCX (Scleraxis) and MKX (Mohawk) are necessary for tendon development [39,40]. SCX activates the expression of *TNMD* (Tenomodulin) which encodes a type II transmembrane glycoprotein [41–43] and *COL1A1* (Collagen 1a1) [44] which encodes the major collagen component of tendons. Here, we tested whether hASC cultured in a 3D type I collagen support ECM and submitted to static uniaxial tension were able to differentiate into tendon cells and potentially form tendon organoids. Analysis of the genetic program during culture of the 3D-hASC constructs indicated that hASCs differentiated towards a tendon phenotype with increased expression of *SCX*, *MKX*, *TNMD* and *COL1A1*. In addition, we analyzed the expression of 9 genes selected among a list of 100 upregulated genes during mouse forelimbs embryonic development, identified by transcriptomic analysis [45]. All of these genes, encoding for transmembrane (*TM4SF1*), cytosolic (*ANXA1*) and ECM (*THBS2*, *DPT*, *DCN*, *POSTN*, *COL6A1* and *COL14A1*) proteins, were expressed at different stages of the 3D-hASC construct culture. This synthesis of ECM components was associated with increased stiffness and reduced relaxation of tendon organoids along the course of their development.

Results

Development of a 3D-culture system using human Adipose Stromal Cells.

We developed a 3D-culture system with primary extracted human Adipose Stromal Cells (hASC). These mesenchymal stem cells were isolated from the stromal vascular fraction of human adipose tissue collected after liposuction surgery [46,47]. In order to mimic tendon development in vitro, we set up a collagen-based 3D cell culture system using the Flexcell bioreactor (Supplementary Figure 1). This technology consists in a holder with 24 cylindrical moulds conferring a homogeneous and regular shape to the constructs [48]. Each mould is perforated with vertical holes through which the vacuum is applied, allowing the silicon elastic surface of the well to acquire the shape of the mould (Figure 1A). At the extremities of each cylinder, two nylon anchor stems allowed the maintenance of static tension in each construct [48] (Figure 1A). After isolation and amplification, hASC were embedded in a 3.5% bovine type I collagen reconstituted matrix and seeded between the two anchor stems. Vacuum was maintained for 2 hours to generate a construct of cylindrical shape. 3D-hASC constructs were than incubated for 48 hours to allow cell development under static tension by condensing the surrounding matrix [36]. Samples were subsequently analysed starting from this timepoint

(which we define as Day 0). Once generated, the 3D-constructs were maintained under static conditions and only subjected to the tension forces exerted between the two anchoring points for 21 days. The distance between the two anchoring points is 2.5cm. On Day 0, constructs exhibited a diameter mean value of 2.08+/-0.08 mm (Figure 1B). Tendon diameter decreased drastically between Day 0 and Day 7 (0.67+/-0.02 mm at Day 7) before to slowly decrease until Day 21 (0.59+/-0.02 mm at Day 14, 0.55+/-0.04 mm at Day 21) (Figure 1B). Notably, considering that the length of the construct is fixed, this corresponds to a volume reduction of the construct of about 15-fold in the course of the 21 Days of culture. Previous studies performed using human dermal fibroblasts (HDF01035) or calf patellar tendon cells embedded in collagen demonstrated that cells generate compaction of collagenous matrix [49,50]. This could explain the reduction in the diameter of 3D-hASC constructs. The total number of cells in the constructs remained stable between Day 0 and Day 21, with a slight increase on Day 4 (Figure 1C). The slight reduction in total cell number between Day 4 and Day 7 in the constructs was not due to apoptosis (Supplementary Figure 2A) but more likely to cell egress from the 3D-hASC constructs (Supplementary Figure 2B). In contrast to 2D-culture system where hASCs exhibited a star shape (Figure 1A), hASC started exhibiting a fusiform, spindle shape, typical of tenocytes and were aligned in the direction defined by the two anchor points. In addition, hASCs started producing type I Collagen as early as Day 0, as seen by immuno-staining (Figure 1D). Finally, the expression of the recognized tendon markers *SCX*, *COL1A1*, *TNMD* and *THBS2* was visualized by in situ hybridization on Day 4 (Figure 1E), suggesting that hASC had initiated a differentiation into tendon cells at this stage.

The Young's modulus of 3D-hASC constructs increased over time.

Organism mobility relies on the ability of tendons to transmit forces from muscles to bones. To accomplish this function, tendons exhibit specific viscoelastic properties, with a Young's modulus much higher than other soft tissues [51,52]. We measured the Young's modulus of 3D-hASC constructs in the course of the 21 Days of construct culture [53]. For that, we used nanoindentation, which consists in probing the mechanical properties of a material at the local scale (micron scale in our case), through the application of controlled deformations on the surface of the sample. To maintain the tendon organoids immobile during the nanoindentation experiments, they were detached from their anchor points and deposited onto a support composed of grooves whose length and diameters were adjusted according to constructs geometry. The support was maintained in a petri dish with agarose gel while 3D-hASC

constructs were fixed to the support using dissection pins inserted through the anchor stems and in the agarose gel (Figure 2A). Indentation was performed by moving the base of the cantilever at a constant speed of 10µm.s^{-1}, with beads whose diameter ranged from about 50 to 100 µm (Fig 2B-C). The relationship between applied force and 3D-hASC construct deformation provides information about 3D-hASC construct mechanical properties. In particular, tissue effective Young's modulus E_{eff} was calculated by fitting the force-indentation curve over a one-micron indentation range using the Hertz model (Figure 2D, see methods). The effective Young's modulus increased significantly during the 21 Days of construct culture starting from 1.3 kPa at Day 0 to 9.2 kPa at Day 21 (Figure 2E). Notably, E_{eff} increased by a factor of about two every seven days. This indicates that this long time-scale stiffening is unlikely to be due to ECM compaction, which occurred almost exclusively during the first week of culture, but rather to the synthesis of specific ECM components.

Developmental tendon marker expression increased in 3D-hASC contstructs over time.

In order to assess whether stiffening of our constructs could correlate with specific molecular programs expressed during tendon differentiation, we next analysed gene expression of recognized and putative tendon markers during 3D-hASC construct culture. The expression levels of the main tendon markers (*SCX*, *MKX*, *TNMD*, *COL1A1*) and tendon genes identified in mouse embryonic limb development (*TM4SF1*, *ANXA1* and *S100A10*) were first analysed by RT-qPCR. Tendon cell differentiation relies on transcription factor gene expression such as *SCX* and *MKX* [39,40]. *SCX* expression was detected, although at low level, both by in situ hybridization and RT-qPCR (Figure 3A-B). *SCX* expression slightly increased up to Day 7, remained constant up to Day 14 and then decreased up to Day 21 (Figure 3B). *MKX* expression was not detected at Day 0 and Day 2, but started to be expressed on Day 4 and increased up to Day 21 (Figure 3B). *MKX* expression was not detected in Day 0 and Day 2 constructs, started to be expressed on Day 4 and increased up to Day 21 (Figure 3B). *TNMD* encodes a transmembrane protein well known as a tendon marker necessary for tenocyte proliferation and tendon maturation in mouse, chicken and human models [41–43]. Interestingly, *TNMD* was expressed in all 3D-hASC constructs on Day 4 but was not detected or at very low levels at the other timepoints (Figure 3C). These expression levels are consistent with the ones of SCX, which is known to control *TNMD* expression.

Beyond these common markers of tendon differentiation, we analysed the expression levels of new markers identified in mouse tendon cells [24]. *TM4SF1* (Transmembrane 4 superfamily

member 1) encodes a cell membrane marker of cancer stem cells [54] which has been identified in mouse tendon cells [24]. In 3D-hASC constructs, *TM4FS1* expression was detected from Day 0 and increased very significantly during construct development (Figure 3C). *ANXA1* (Annexin A1) encodes a cytosolic Ca^{2+}-regulated phospholipid-binding protein involved in cell membrane formation, actin cytoskeleton rearrangement and which exhibits anti-inflammatory properties in tendon cells after injury [55]. *ANXA1* expression increased during mouse embryonic limb tendon development [24]. In contrast, during 3D-hASC construct development, *ANXA1* expression first decreased on Day 2 and slightly increased on Day 21 (Figure 3D). *S100A10* encodes a member of the S100 family of cytosolic Ca^{2+}-binding proteins which has lost the ability to bind Ca^{2+} and interacts with Annexins [56]. *S100A10* was identified as a top gene expressed during mouse tendon differentiation [24]. Unlike mouse, *S100A10* expression level was stable in 3D-hASC constructs until Day 14, and slightly decreased between Day 14 and Day 21 (Figure 3D).

Finally, we observed that, although hASCs were capable of differentiating into adipocytes and osteocytes in 2D culture, human tendon constructs produced from these stem cells did not contain adipocytes or osteocytes (Supplementary Figure 2).

In summary, we demonstrated that our 3D-hASC constructs triggered the tendon differentiation program, with genes encoding the transcription factors *SCX* and *MKX* upregulated until day 14, while genes encoding the transmembrane proteins *TNMD* and *TM4SF1* showed increased expression until days 7 and 21 respectively, and the gene encoding the cytosolic protein *ANXA1* was upregulated by day 21 only. We next tested whether this activation of the tendon differentiation program was accompanied by an increase in ECM synthesis during tendon constructs culture.

Extracellular matrix gene expression was correlated with changes in visco-elastic properties of 3D-hASC constructs.

Tendon stiffness relies on the synthesis of a dense and organized extracellular matrix generated by tendon cells. We thus analysed the expression of collagens and fibrillogenic proteins during tendon construct development. Type-I collagen is the most abundant protein present in tendons. The non-fibrillar collagen COL6A1 (Collagen 6a1) necessary for collagen fibrillogenesis [57] and the fibril-associated collagen with interrupted triple helices (FACIT) COL14A1 (Collagen 14a1) [58] are up-regulated during mouse embryonic tendon development [24]. In human tendon constructs, *COL1A1*, *COL6A3 and COL14A1* expression was detected on Day 0,

increased until Day 7 and remained elevated and higher at Day 21 compared to Day 0 (Figure 4A-B). DPT (Dermatopontin) [59–61], DCN (Decorin) [62], POSTN (Periostin) [63] and THBS2 are involved in collagen fibrillogenesis and cell-matrix adhesion. Their mRNA expression was significantly increased during human tendon construct development (Figure 4C-D). The strong increase of ECM gene expression during tendon construct development was consistent with the increase of effective Young's modulus (Figure 2E). In addition, the increased expression of *DPT*, *DCN*, *POSTN* and *THBS2*, regulators of ECM network, also suggested that the structure and organisation of the ECM was modified during the course of tendon construct formation. We thus tested whether ECM synthesis was accompanied with a modification of the visco-elastic properties of tendon constructs along time. To do this, we carried out stress relaxation experiments using nanoindentation (Figure 5). In particular, we calculated the percentage of relaxation r_{relax} from the peak force F_{max} measured at the end of the indentation ramp and the force $F_{t=10s}$ measured after 10 seconds of relaxation ($r_{relax} = (F_{max}-F_{t=10s})/F_{max}$). The higher this ratio is, the more liquid-like the material. Oppositely, a smaller ratio indicates more solid, elastic-like visco-elastic properties. On Day 0, the percentage of relaxation was 35% and decreased along time down to 24% on Day 21 (Figure 5E), in parallel with the increase of ECM synthesis. We conclude that the tendon constructs acquire solid-like properties, consistent with the synthesis of ECM and its cross-linkers during the time course of the cultures.

hASC differentiated towards a tendon phenotype and organize into two cell populations. Transverse sections of 3D-hASC constructs revealed that cell organisation within the constructs evolved along time forming two populations, one at the centre and the other at the periphery (Figure 6A), reminiscent of peritenon surrounding tendon proper [64]. From Day 2, a population of cells assembled at the periphery of 3D-hASC constructs. and formed a ring composed of 3 to 4 layers of cells from Day 4 to Day 21. Cell density at the ring and the centre is maintained from Day 4 to Day 21 (Figure 6B). A Phalloidin staining showed that the peripheral cell population formed a ring composed of 3 to 4 layers of cells from Day 4 to Day 21, which was separated from the central region by a sharp interface (Figure 6A). As opposed to cells in the centre, which aligned parallel to the long axis of the cylinder (Fig. 1D), ring cells spread tangential to the surface of the construct. As opposed to cells in the centre, which aligned parallel to the long axis of the cylinder (Fig. 1F), ring cells spread tangential to the surface of the construct. Cell density in the ring and in the central region was constant from Day 4 to Day 21 (Figure 6B). Cell density in the ring and in the central region was constant from Day 4 to Day 21 (Figure 6B). Interestingly, ECM gene expression evolved along time in the two cell

populations in a different manner (Figure 4A,D). As revealed by in situ hybridization, *COL1A1* expression showed elevated expression from Day 7 and until Day 14 in both centre and ring cells of the 3D-hASC construct (Figure 4A). However, at Day 21, *COL1A1* was more expressed in centre cells compared to ring cells (Figure 4A). By contrast, *THBS2* was visualized in both centre and ring 3D-hASC construct cells along the 21 days of culture (Figure 4D).

Altogether, this demonstrates that 3D-hASC constructs self-organize into two different cell populations with different shapes, gene expression and localization.

Discussion

This study showed that hASCs embedded in collagen hydrogel and submitted to static tension forces were capable of forming a 3D-constructs with a tendon phenotype, which reproduced tendon organization. After 21 days of cell culture, tendon constructs expressed high levels of ECM components, correlated with a Young's modulus value comprised between 5.6 and 18.3 kPa (Figure 2E). Interestingly, measurement of nanoscale elastic modulus of chick embryonic calcaneus tendons calculated similarly through Hertz contact theory gave similar results (5-17 kPa) [65,66], which suggests that our tendon construct system could mimic embryonic tendon development.

SCX is expressed from E9.5 in mouse forelimbs [39] and early postnatal period [67]. *SCX* expression is next dramatically decreased from the age of 3 to 4 month in mouse [68]. *MKX* mRNA expression is slightly detectable in mouse tendon at E12.5, after the emergence of SCX expression (E9.5) [40]. *MKX* mRNA expression is then elevated at E13.5 and E14.5, when tendon progenitors undergo condensation and differentiation [40]. In our system, *SCX* expression was detected from Day 0 to Day 4 and decreases from Day 14, suggesting that SCX was no longer required for tendon differentiation at this step (Figure 3A-B). Interestingly, *MKX* was not detected before Day 4 and was expressed in all tendon constructs at Day 14, which suggests that SCX and MKX act in a sequential manner during tendon constructs formation (Figure 3B), as observed during mouse tendon development [40]. *TNMD* encodes a transmembrane protein known as a tendon marker necessary for tenocyte proliferation and collagen fibrilmaturation in newborn mice [41]. In our system, *TNMD* exhibited a transitory expression detected in all constructs at Day 4 only (Figure 1G and Figure 3C). Interestingly, expression of *TNMD* at Day 4 coincides with a significant increase of cell number in tendon constructs (Figure 1E), suggesting that TNMD promoted proliferation of tendon cells in our system. TM4SF1 is known as involved in cancer development through the promotion of cancer

cell proliferation, metastasis and angiogenesis [69]. We previously observed that *TM4SF1* expression was activated during mouse tendon limb development [24] and confirmed in this study that *TM4SF1* was also significantly activated in human tendon construct cells (Figure 3C). *TM4SF1* might thus be considered as a new tendon marker. In contrast, the cytosolic proteins ANXA1 and S100A10 that showed an increased expression during mouse limb tendon development [24] were highly expressed in human tendon constructs but their expression levels remain globally constant, indicating that tendon differentiation from hASC does not rely on *ANXA1* or *S100A10* expression (Figure 3D). In summary, human tendon constructs express the genetic programs involved in tendon development and ECM synthesis. The analysis of ECM components expression during human tendon construct development confirmed that hASC were differentiating into tenocytes which exhibit high level of ECM protein expression (Figure 4A-D). The elevated expression of ECM coding genes was associated with a significant increase of tendon construct stiffness (Figure 2E) and reduction of tendon construct relaxation (Figure 5E), demonstrating a link between ECM gene expression and visco-elastic properties of constructs.

During tendon construct formation, cells self-organized in two separate populations, one being at the centre of the construct and the other forming a ring at the periphery (Figure 6). This could be an effect of the geometry of the constructions defined by the anchoring points, which may orient cell shape and ECM. These mechanical cues could then feedback on gene expressions via mechano-sensing [70]. Interestingly, we observed the same cellular organization in vivo in mouse embryonic forelimb tendons [45] and cells surrounding tendons have also been described in post-natal rat and mice [71]. These organizations, like the one we observed in our system, might be the precursors of the peritenon surrounding tendons in adult.

In summary, our system meets the 3 criteria that define organoids: 1) it exhibits several cell types with the ring and centre cells; 2) the system shows a potential for organ function, as shown from increased stiffness and ECM synthesis characteristic of tendon in development, and 3) the construct organizes by self-organisation within a minimal environment: static tension and type I collagen support.

The consequences of dynamic uniaxial mechanical loading have been tested on 3D-tendon organoids produced from various sources of rodent or human mesenchymal stem cells [28]. Multiple loading conditions, from 1% to 20% elongation at the frequency of 0.25 Hz to 1 Hz various frequencies have been tested on tendon constructs with contradictory results as to their beneficial effect on tendon formation [17,28]. While mechanical loading has been shown to

enhance the expression of type I and type III collagen genes, it is also accompanied by a significant increase in apoptosis [17,28]. Furthermore, it has been shown that mechanical stimulation does not improve the mechanical properties of tendon organoids, including Young's modulus [17]. Although hASC seem to exhibit lower osteogenic potential in vitro compared to hBMMSC [72], mechanical stretching on 2D-cultures hASC subjected to 10% elongation at 0.5 Hz promoted unwanted osteogenic marker expression in hASC [73]. The next step will be to determine whether it is possible to establish dynamic mechanical loading conditions that would improve the expression of tendon differentiation genetic programs, ECM production and tendon physical properties, compared with uniaxial static conditions.

This study has developed a robust strategy using human cells that mimics tendon development. It should pave the way for regenerative medicine once this technology is effectively scaled up.

Experimental procedures

Cell sample collection

Human abdominal subcutaneous adipose tissues were obtained from healthy donors after liposuction surgery (AP-HP Saint-Antoine Hospital, Paris, France). Human Adipose stromal cells (hASC) were isolated from 3 healthy donors (one woman and two men).

All donors provided their written, informed consent to the use of their tissue specimens for research purposes. The study was performed in compliance with the principles of the Declaration of Helsinki and was approved by an institutional review board. The study was approved by the French regulatory authorities (Codecoh DC2023-5617). Cells were cryopreserved in 2mL cryotubes (2x106 cells per vial) stored in liquid nitrogen tanks.

Cell amplification

For each experiments, cell vials were thawed 2-3 min in a 37°C water bath and transferred in T25 cell culture flasks (Gibco) with 5ml of hASC culture medium containing Minimum Essential Mediun (αMEM; Gibco; ref 22571-020) complemented with 10% Fetal Calf Serum (FCS; Gibco; ref 35-079-CV), 1% HEPES (1M, sigma; ref H0887-100ml), 1% glutamine (100X, 200mM, Gibco; ref 25030-024), 1% Penicillin/Streptomycin (Gibco; ref 15140-122) and 2.5 ng/mL FGF2 (PeproTech, Rocky Hill, NJ; ref 100-18B). Confluent cells were submitted to 2 passages, at 1:9 and 1:3 ratio. For each passage, we used 0.05% Trypsin (Gibco; ref 25300-054) for 5 minutes.

Preparation of tendon constructs

Tendon constructs were prepared as described in Scott et al., 2011[74]. Briefly, sub confluent cells were detached in 5 ml of 0.05% trypsin for 5 minutes, then suspended with hASC culture medium (described below) and counted with a Malassez counting chamber. 16.2 million cells (600,000 cells per tendon construct) were centrifuged at 1200 rpm for 5 minutes and resuspended in 4.05 mL of Type I collagen solution containing 70% Purecoll (Sigma-Aldritch, Oakville, Canada; ref 5074-35ml), 10% FCS and 20% αMEM brought to 7.4 pH with 0.1 N NaOH immediately before use. 150 µl of hASC-collagen mix was pipetted into each well of an untreated TissueTrain© plate (FlexCell International, Hillsborough NC; ref TTLC-4001C) according to the manufacturer's instructions. The collagen hydrogel was allowed to set for 2 hours, and the tendon constructs were covered with 2 ml of hASC culture medium completed with 0.25 mM ascorbic acid. The medium was replaced every 2-3 Days.

Nanoindentation measurements

Live tendon constructs were detached from their anchor points and immediately fixed onto a 3D-printed support. To avoid sliding of the construct during mechanical testing, the support was designed with three half-cylindrical grooves at its surface whose diameters were adjusted to the typical tendon constructs diameters. In order to conserve the original length of the tendon construct, the length of the support was also calibrated to the original distance between the anchor points in the bioreactor. The support was then embedded in an agarose gel in a Petri dish, and the samples were immersed in culture medium. Mechanical testing was performed at room temperature, using a Piuma nano-indenter (Optics11 Life), as described in the main text. Samples were positioned under the probe using a magnifying glass. Five measurements were performed along the tendon construct length and their mean value was calculated to extract effective Young's modulus and percentage of stress relaxation for each sample.

The effective Young's modulus E_{eff} was calculated from a fit of the force versus indentation curve over a 1µm indentation course and using a Hertzian contact model as follows:

$$F = \frac{4}{3} E_{eff} \sqrt{R_i} \cdot h^{3/2}$$

where F is the force, Ri the tip radius, and h the indentation.

Tendon construct sections

Tendon constructs were fixed in 1% paraformaldehyde (PFA, Gibco Sigma; ref 158127-100G) overnight at 4°C, washed in 1X PBS (Gibco; ref :14190-094) and put in a 15% sucrose solution at 4°C for 3 Days. Before inclusion, tendon constructs were incubated in a 7,5% gelatin-15% sucrose solution in a 37°C water bath for 1 hour. Included tendon constructs were then frozen at -80°C in isopentane for 1 minute and 12µm cryosections were generated with a CM3050 S Cryostat (Leica Biosystems).

COL1A1 immunostaining

Tendon construct 12µm cryosections were subject to a standard immunofluorescence protocol using human COL1A1 (Abcam; ref ab260043) primary antibody at 1:100 dilution and Goat anti-Rabbit IgG (H+L) Cross-Adsorbed, Alexa Fluor™ 488 (Invitrogen/ ThermoFisher scientific; ref A11008) secondary antibody at 1:200 dilution. Finally, sections were stained with DAPI (Sigma-Aldrich; ref D9542) to visualize cell nuclei and phalloidin (Alexa Fluor Phalloidin, Invitrogen/ Thermo Fisher scientific; ref A12380) to visualize cytoskeletal F-actin. Fluorescent images were captured using a Zeiss Axio Observer Z1 microscope equipped with a Zeiss Apotome 2 and an Axiocam 506 monochrome camera.

In situ hybridization

Tendon construct 12µm cryosections were subject to a standard in situ hybridization protocol [75]. *SCX, TNMD, COL1A1* and *THBS2* probes were generated using a Roboprobe kit (Promega; ref P1460), according to manufacturer's instructions. Images were captured using a Nanozoomer SQ Digital Slide Scanner with NDP.view2 software (Hamamatsu Photonics). The primers used for probe synthesis are listed in Supplementary table 1.

RNA isolation

Tendon constructs were put in 500µL RLT (Qiagen; ref 74106) and homogenized using a mechanical disruption device (Lysing Matrix A, Fast Prep MP1, 4 × 30 s, 6 $m.s^{-1}$). Total RNA was isolated using the RNeasy mini kit (Qiagen; ref 74106), according to the manufacturer's instructions, including a 15 min of DNase I (Qiagen; ref 79254) treatment.

Reverse-Transcription and quantitative real time PCR

Total RNAs extracted from tendon constructs were Reverse Transcribed using the High Capacity Retro-transcription kit (Applied Biosystems; ref 4387406). Quantitative PCR analyses

were performed using primers listed in Supplementary Table 1 and SYBR Green PCR Master Mix (Applied Biosystems; ref 4385614). The relative mRNA levels were calculated using the $2^{-\Delta\Delta Ct}$ method [76]. The cycle threshold (C_T) corresponds to the number of cycles required for the fluorescent signal to cross the threshold (to exceed background level).The C_Ts were obtained from C_T normalized to *YWHAZ* level in each sample. The primers used for RT-qPCR experiments are listed in Supplementary table 1.

Statistical analyses

Data was analysed using the non-parametric Mann-Whitney test with Graphpad Prism V10. Results are shown as means ± standard deviations. The p-values are indicated either with the value or with * or #.

Funding sources

This work was supported by the CNRS, INSERM, Sorbonne University and ANR_TENORS.

Acknowledgements

We would like to thank Mathieu Hautefeuille for proofreading the manuscript.

Figure Legends

Figure 1: Generation of tendon constructs using a Flexcell bioreactor. A) Human adipose stromal cells are isolated from lipoaspirates and amplified before seeding. The cells are embedded in a 3.5% collagen hydrogel and deposited between the two anchor points. The polymerization is performed by maintaining the vacuum and at 37°C for 2 hours. The vacuum is then broken and the tendon constructs are kept in the incubator for 48 hours before starting the experiments. Scale bar 100µm. B) Tendon constructs were cultured for 21 days and diameters were measured from constructs at Day 0 (n=11), Day 7 (n=15), Day 14 (n=14) and Day 21 (n=19). Each color represents a set of experiments. 4 independent experiments were performed with 3<n<8 biological replicates for each experiment. The p-values were obtained using the Mann-Whitney test. Asterisks * indicate the p-values of tendon construct diameter compared to each following stage, * P<0.05, ****P<0.001. Scale bars 500µm. C) Tendon construct total cell number was counted at Day 0 (n=18), Day 2 (n=12), Day 4 (n=10), Day 7 (n=15), Day 14 (n=9) and Day 21 (n=9). Each color represents a set of experiments. 6 independent experiments were performed with n ≥ 3 biological replicates for each experiment. The p-values were obtained using the Mann-Whitney test. Asterisks * indicate the p-values of tendon construct cell number compared to each following stage, * P<0.05, ***P<0.001, ****P<0.0001, D) Longitudinal sections of tendon constructs were performed on Day 0 and Day 2 and stained with DAPI/Phalloidin to visualize cell shape and COL1A1 antibody. E) The expression of *SCX, TNMD, COL1A1 and THBS2* was visualized by in situ hybridization on Day 4 tendon constructs transversally cryo-sectioned. 12 µm sections were hybridized with the DIG-labeled antisense probes for *SCX, TNMD, COL1A1 and THBS2*. Scale bars: 200 µm

Figure 2: Tendon construct Young's modulus increased along time. A) Tendon constructs are fixed on a 3D-printed support maintained in agarose gel. Tendon constructs are placed in an appropriate channel according to their diameter and fixed using dissection pins inserted into the anchor stems and agarose. B) The one-piece optical probe of the nanoindenter is composed of an optical fiber, a cantilever and a spherical tip. After an approach phase, the tip touches the sample and indent it. The cantilever bending is detected by the optical fiber. C) Force as a function of cantilever base displacement for a typical indentation. Inset: Cantilever base displacement is applied at constant rate of 10µm.s-1. D) Force as a function of indentation for a typical indentation curve. Hertz contact fit (red) is applied over a 1 µm indentation. E) Evolution of effective Young's modulus along culture time. Each dot represents the mean of five measurements performed on one 3D-hASC construct. Indentation experiments were performed at Day 0 (n=17), Day 7 (n=17), Day 14 (n=13) and Day 21 (n=14). Each color represents a set of experiments. 5 independent experiments were performed with 3<n<8 biological replicates for each experiment. The p-values were obtained using the Mann-Whitney test. Asterisks * indicate the p-values of Young's modulus levels (kPa) compared to each following stage, ***P<0.001, ****P<0.0001.

Figure 3: Tendon differentiation programs were expressed during human tendon construct formation in a time-dependent manner. A) Tendon constructs at Day 0, Day 7, Day 14 and Day 21 were transversally cryo-sectioned. 12 µm sections were hybridized with the DIG-labeled antisense probes for *SCX*. Scale bars: 30µm. After 0, 2, 4, 7, 14 and 21 Days of culture, tendon constructs were used for mRNA purification. mRNA samples were analysed by RT-qPCR for B) Transcription factor coding genes *SCX* and *MKX*. C) mRNA expression levels of transmembrane protein coding genes *TNMD* and *TM4FS1*. D) mRNA expression levels of cytosolic protein coding genes *ANXA1* and *S100A10*. Transcripts are shown relative to the level of *YWHAZ* transcripts. The relative mRNA levels were calculated using the $2^{-\Delta\Delta Ct}$ method, with control being normalized to 1. Each color represents a set of experiments. 8 independent experiments were performed with $14 < n < 29$ 3D-hASC construct generated for each step (n=29 at Day 0, n=19 at Day 2, n=18 at Day 4, n=25 at Day 7, n=17 at Day 14 and n=16 at Day 21). Error bars represent the mean + standard deviations. The p-values were obtained using the Mann-Whitney test. Asterisks * indicate the p-values of gene expression levels in tendon constructs compared to the first Day of gene detection *P<0.05, **P<0.01, *** P<0.001, **** P<0.0001.

Figure 4: Extra-cellular matrix gene expression was highly increased during tendon construct development. A) Tendon constructs at Day 0, Day 7, Day 14 and Day 21 were transversally cryo-sectioned. 12 µm sections were hybridized with the DIG-labeled antisense probes for *COL1A1*. Scale bars 30µm. After 0, 2, 4, 7, 14 and 21 Days of culture, tendon constructs were used for mRNA purification. B) mRNA expression levels of extracellular matrix protein coding genes *COL1A1*, *COL6A3*, and *COL14A1* were analysed by RT-qPCR. C) mRNA expression levels of extracellular matrix fibrillogenic protein coding genes *DPT*, *DCN*, *POSTN* and D) *THBS2*. Transcripts are shown relative to the level of *YWHAZ* transcripts. The relative mRNA levels were calculated using the $2^{-\Delta\Delta Ct}$ method, with control being normalized to 1. Each color represents a set of experiments. 8 independent experiments were performed with $14 < n < 29$ tendon construct generated for each step (n=29 at Day 0, n=19 at Day 2, n=18 at Day 4, n=25 at Day 7, n=17 at Day 14 and n=16 at Day 21). Error bars represent the mean + standard deviations. The p-values were obtained using the Mann-Whitney test. Asterisks * indicate the p-values of gene expression levels in tendon constructs compared to the first Day of gene detection *P<0.05, **P<0.01, *** P<0.001, **** P<0.0001. Tendon constructs at Day

0, Day 7, Day 14 and Day 21 were transversally cryo-sectioned. 12 µm sections were hybridized with the DIG-labeled antisense probes for *THBS2*. Scale bars 30µm.

Figure 5: Visco-elastic properties of human tendon constructs change along time. A) Schematic of a force relaxation experiment. In open loop, the base of the cantilever is fixed while relaxation takes place. B) Typical curve showing force as a function of indentation during loading, relaxation and unloading phase. Inset: Indentation as a function of time. C) Force as a function time. Force peaks at a value Fmax and reaches is close to a plateau after 10s of relaxation. Frelax is defined as the force at this instant. E) Percentage of stress relaxation ((Fmax – Ft=10 sec) / Fmax)) x100 during the first 10 seconds of relaxation, after different periods of cell culture. Each dot represents the mean of five measurements performed on one 3D-hASC construct. Indentation experiments were performed at Day 0 (n=17), Day 7 (n=17), Day 14 (n=13) and Day 21 (n=14). Each color represents a set of experiments. 5 independent experiments were performed with 3<n<8 biological replicates for each experiment. The p-values were obtained using the Mann-Whitney test. Asterisks * indicates the p-value of tendon construct relaxation at Day 7, Day 14 and Day 21 versus Day 0; *P<0.05. # indicates the p-value of tendon construct relaxation at Day 7 versus Day 14; # P<0.05.

Figure 6: Cellular organization in 3D engineered tendons. A) Transverse sections of tendon constructs were performed on Day 0, Day 2, Day 4, Day 7, Day 14 and Day 21 of culture and stained with DAPI/Phalloidin to visualize cell organization within the tendon constructs. From Day 2, tendon constructs are composed of two cell populations, one at the centre and the other at the periphery, forming a ring. B) Cell density was counted at the centre and the ring of tendon constructs at Day 0 (n=18), Day 2 (n=12), Day 4 (n=10), Day 7 (n=15), Day 14 (n=12) and Day 21 (n=9). The p-values were obtained using the Mann-Whitney test compared to each following stage. Asterisks * indicate the p-values of cell number at the centre, *** P <0.001, **** P<0.0001; # indicate the p-values of cell number at the ring, #### P <0.0001; Scale bars 100µm.

References

[1] C.N. Riggin, T.R. Morris, L.J. Soslowsky, Tendinopathy II: Etiology, Pathology, and Healing of Tendon Injury and Disease, Elsevier Inc., 2015. https://doi.org/10.1016/B978-0-12-801590-2.00005-3.

[2] N.J. Lemme, N.Y. Li, S.F. DeFroda, J. Kleiner, B.D. Owens, Epidemiology of Achilles Tendon Ruptures in the United States: Athletic and Nonathletic Injuries From 2012 to 2016, Orthop J Sports Med 6 (2018) 1–7. https://doi.org/10.1177/2325967118808238.

[3] C. Wang, Z. Jiang, R. Pang, H. Zhang, H. Li, Z. Li, Global trends in research of achilles tendon injury/rupture: A bibliometric analysis, 2000–2021, Front Surg 10 (2023). https://doi.org/10.3389/fsurg.2023.1051429.

[4] G. Nourissat, F. Berenbaum, D. Duprez, Tendon injury: From biology to tendon repair, Nat Rev Rheumatol (2015). https://doi.org/10.1038/nrrheum.2015.26.

[5] M.L. Bayer, C.Y.C. Yeung, K.E. Kadler, K. Qvortrup, K. Baar, R.B. Svensson, S. Peter Magnusson, M. Krogsgaard, M. Koch, M. Kjaer, The initiation of embryonic-like collagen fibrillogenesis by adult human tendon fibroblasts when cultured under tension, Biomaterials 31 (2010) 4889–4897. https://doi.org/10.1016/j.biomaterials.2010.02.062.

[6] A. Herchenhan, M.L. Bayer, R.B. Svensson, S.P. Magnusson, M. Kjær, In vitro tendon tissue development from human fibroblasts demonstrates collagen fibril diameter

growth associated with a rise in mechanical strength, Developmental Dynamics 242 (2013) 2–8. https://doi.org/10.1002/dvdy.23896.

[7] A. Herchenhan, F. Dietrich-Zagonel, P. Schjerling, M. Kjaer, P. Eliasson, Early Growth Response Genes Increases Rapidly After Mechanical Overloading and Unloading in Tendon Constructs, J Orthop Res 38 (2020) 173—181. https://doi.org/10.1002/jor.24513.

[8] A. Giannopoulos, R.B. Svensson, K.M. Heinemeier, P. Schjerling, K.E. Kadler, D.F. Holmes, M. Kjaer, S. Peter Magnusson, Cellular homeostatic tension and force transmission measured in human engineered tendon, J Biomech 78 (2018) 161–165. https://doi.org/10.1016/j.jbiomech.2018.07.032.

[9] A.J. Friedenstein, K. V Petrakova, A.I. Kurolesova, G.P. Frolova, Heterotopic of bone marrow. Analysis of precursor cells for osteogenic and hematopoietic tissues, Transplantation 6 (1968) 230–247.

[10] B.M. Abdallah, M. Kassem, The use of mesenchymal (skeletal) stem cells for treatment of degenerative diseases: current status and future perspectives, J Cell Physiol 218 (2009) 9–12. https://doi.org/10.1002/jcp.21572.

[11] A.J. Friedenstein, R.K. Chailakhyan, U. V Gerasimov, Bone marrow osteogenic stem cells: in vitro cultivation and transplantation in diffusion chambers, Cell Tissue Kinet 20 (1987) 263–272.

[12] R.K. Jaiswal, N. Jaiswal, S.P. Bruder, G. Mbalaviele, D.R. Marshak, M.F. Pittenger, Adult human mesenchymal stem cell differentiation to the osteogenic or adipogenic lineage is regulated by mitogen-activated protein kinase, J Biol Chem 275 (2000) 9645–9652.

[13] M.F. Pittenger, A.M. Mackay, S.C. Beck, R.K. Jaiswal, R. Douglas, J.D. Mosca, M.A. Moorman, D.W. Simonetti, S. Craig, D.R. Marshak, Multilineage potential of adult human mesenchymal stem cells, Science 284 (1999) 143–147.

[14] C.K. Kuo, R.S. Tuan, Mechanoactive tenogenic differentiation of human mesenchymal stem cells, Tissue Eng Part A 14 (2008) 1615–1627. https://doi.org/10.1089/ten.tea.2006.0415.

[15] Z. Kapacee, C.Y.C. Yeung, Y. Lu, D. Crabtree, D.F. Holmes, K.E. Kadler, Synthesis of embryonic tendon-like tissue by human marrow stromal/mesenchymal stem cells requires a three-dimensional environment and transforming growth factor β3, Matrix Biology 29 (2010) 668–677. https://doi.org/10.1016/j.matbio.2010.08.005.

[16] C.F. Hsieh, Z. Yan, R.G. Schumann, S. Milz, C.G. Pfeifer, M. Schieker, D. Docheva, In vitro comparison of 2D-cell culture and 3D-cell sheets of scleraxis-programmed bone marrow derived mesenchymal stem cells to primary tendon stem/progenitor cells for tendon repair, Int J Mol Sci 19 (2018). https://doi.org/10.3390/ijms19082272.

[17] H. Park, S.N. Nazhat, D.H. Rosenzweig, Mechanical activation drives tenogenic differentiation of human mesenchymal stem cells in aligned dense collagen hydrogels, Biomaterials 286 (2022) 121606. https://doi.org/10.1016/j.biomaterials.2022.121606.

[18] P.A. Zuk, Tissue engineering craniofacial defects with adult stem cells? Are we ready yet?, Pediatr Res 63 (2008) 478–486. https://doi.org/10.1203/PDR.0b013e31816bdf36.

[19] J.M. Gimble, A.J. Katz, B.A. Bunnell, Adipose-derived stem cells for regenerative medicine, Circ Res 100 (2007) 1249–1260. https://doi.org/10.1161/01.RES.0000265074.83288.09.

[20] B. Lindroos, R. Suuronen, S. Miettinen, The potential of adipose stem cells in regenerative medicine, Stem Cell Rev 7 (2011) 269–291. https://doi.org/10.1007/s12015-010-9193-7.

[21] P.A. Zuk, M. Zhu, P. Ashjian, D.A. De Ugarte, J.I. Huang, H. Mizuno, Z.C. Alfonso, J.K. Fraser, P. Benhaim, M.H. Hedrick, Human Adipose Tissue Is a Source of Multipotent Stem Cells, Mol Biol Cell 13 (2002) 4279–4295. https://doi.org/10.1091/mbc.E02.

[22] P. Zuk, Adipose-Derived Stem Cells in Tissue Regeneration: A Review, Int Sch Res Notices 2013 (2013) e713959. https://doi.org/10.1155/2013/713959.

[23] M.-J. Guerquin, B. Charvet, G. Nourissat, E. Havis, O. Ronsin, M.-A. Bonnin, M. Ruggiu, I. Olivera-Martinez, N. Robert, Y. Lu, K.E. Kadler, T. Baumberger, L. Doursounian, F. Berenbaum, D. Duprez, Transcription factor EGR1 directs tendon differentiation and promotes tendon repair, Journal of Clinical Investigation 123 (2013). https://doi.org/10.1172/JCI67521.

[24] E. Havis, M.-A. Bonnin, I. Olivera-Martinez, N. Nazaret, M. Ruggiu, J. Weibel, C. Durand, M.-J. Guerquin, C. Bonod-Bidaud, F. Ruggiero, R. Schweitzer, D. Duprez, Transcriptomic analysis of mouse limb tendon cells during development, Development (Cambridge) 141 (2014). https://doi.org/10.1242/dev.108654.

[25] K. Otabe, H. Nakahara, A. Hasegawa, T. Matsukawa, F. Ayabe, N. Onizuka, M. Inui, S. Takada, Y. Ito, I. Sekiya, T. Muneta, M. Lotz, H. Asahara, Transcription factor mohawk controls tenogenic differentiation of bone marrow mesenchymal stem cells in vitro and in vivo, Journal of Orthopaedic Research 33 (2015) 1–8. https://doi.org/10.1002/jor.22750.

[26] H.Y. Nam, H.R.B. Raghavendran, B. Pingguan-Murphy, A.A. Abbas, A.M. Merican, T. Kamarul, Fate of tenogenic differentiation potential of human bone marrow stromal cells by uniaxial stretching affected by stretch-activated calcium channel agonist gadolinium, PLoS One 12 (2017) 1–20. https://doi.org/10.1371/journal.pone.0178117.

[27] L. Gaut, M.A. Bonnin, C. Blavet, I. Cacciapuoti, M. Orpel, M. Mericskay, D. Duprez, Mechanical and molecular parameters that influence the tendon differentiation potential of C3H10T1/2 cells in 2D- And 3D-culture systems, Biol Open 9 (2020) 1–13. https://doi.org/10.1242/bio.047928.

[28] T. Wang, P. Chen, M. Zheng, A. Wang, D. Lloyd, T. Leys, Q. Zheng, M.H. Zheng, In vitro loading models for tendon mechanobiology, Journal of Orthopaedic Research 36 (2018) 566–575. https://doi.org/10.1002/jor.23752.

[29] G. Yang, B.B. Rothrauff, H. Lin, R. Gottardi, P.G. Alexander, R.S. Tuan, Enhancement of tenogenic differentiation of human adipose stem cells by tendon-derived extracellular matrix, Biomaterials 34 (2013) 9295–9306. https://doi.org/10.1016/j.biomaterials.2013.08.054.

[30] T. Wang, C. Thien, C. Wang, M. Ni, J. Gao, A. Wang, Q. Jiang, R.S. Tuan, Q. Zheng, M.H. Zheng, 3D uniaxial mechanical stimulation induces tenogenic differentiation of tendon-derived stem cells through a PI3K/AKT signaling pathway, FASEB Journal 32 (2018) 4804–4814. https://doi.org/10.1096/fj.201701384R.

[31] L. Gaut, M.A. Bonnin, C. Blavet, I. Cacciapuoti, M. Orpel, M. Mericskay, D. Duprez, Mechanical and molecular parameters that influence the tendon differentiation potential of C3H10T1/2 cells in 2D- And 3D-culture systems, Biol Open 9 (2020) 1–13. https://doi.org/10.1242/bio.047928.

[32] D. Jaiswal, L. Yousman, M. Neary, E. Fernschild, B. Zolnoski, S. Katebifar, S. Rudraiah, A.D. Mazzocca, S.G. Kumbar, Tendon tissue engineering: Biomechanical considerations, Biomedical Materials (Bristol) 15 (2020). https://doi.org/10.1088/1748-605X/ab852f.

[33] J. Garvin, J. Qi, M. Maloney, A.J. Banes, Novel System for Engineering Bioartificial Tendons and Application of Mechanical Load, Tissue Eng 9 (2003) 967–979. https://doi.org/10.1089/107632703322495619.

[34] T. Wang, C. Thien, C. Wang, M. Ni, J. Gao, A. Wang, Q. Jiang, R.S. Tuan, Q. Zheng, M.H. Zheng, 3D uniaxial mechanical stimulation induces tenogenic differentiation of tendon-derived stem cells through a PI3K/AKT signaling pathway, FASEB Journal 32 (2018) 4804–4814. https://doi.org/10.1096/fj.201701384R.

[35] S. Ruiz-Alonso, M. Lafuente-Merchan, J. Ciriza, L. Saenz-del-Burgo, J.L. Pedraz, Tendon tissue engineering: Cells, growth factors, scaffolds and production techniques, Journal of Controlled Release 333 (2021) 448–486. https://doi.org/10.1016/j.jconrel.2021.03.040.

[36] A. Scott, P. Danielson, T. Abraham, G. Fong, A. V. Sampaio, T.M. Underhill, Mechanical force modulates scleraxis expression in bioartificial tendons, Journal of Musculoskeletal Neuronal Interactions 11 (2011) 124–132.

[37] G. Yang, B.B. Rothrauff, H. Lin, R. Gottardi, P.G. Alexander, R.S. Tuan, Enhancement of tenogenic differentiation of human adipose stem cells by tendon-derived extracellular matrix, Biomaterials 34 (2013) 9295–9306. https://doi.org/10.1016/j.biomaterials.2013.08.054.

[38] J. Burk, A. Plenge, W. Brehm, S. Heller, B. Pfeiffer, C. Kasper, Induction of Tenogenic Differentiation Mediated by Extracellular Tendon Matrix and Short-Term Cyclic Stretching, Stem Cells Int 2016 (2016). https://doi.org/10.1155/2016/7342379.

[39] R. Schweitzer, J.H. Chyung, L.C. Murtaugh, A.E. Brent, V. Rosen, E.N. Olson, A. Lassar, C.J. Tabin, Analysis of the tendon cell fate using Scleraxis, a specific marker for tendons and ligaments, Development 128 (2001) 3855–3866. https://doi.org/10.1242/dev.128.19.3855.

[40] H. Liu, S. Zhu, C. Zhang, P. Lu, J. Hu, Z. Yin, Y. Ma, X. Chen, H. OuYang, Crucial transcription factors in tendon development and differentiation: Their potential for tendon regeneration, Cell Tissue Res 356 (2014) 287–298. https://doi.org/10.1007/s00441-014-1834-8.

[41] D. Docheva, E.B. Hunziker, R. Fässler, O. Brandau, Tenomodulin is necessary for tenocyte proliferation and tendon maturation, Mol Cell Biol 25 (2005) 699–705. https://doi.org/10.1128/MCB.25.2.699-705.2005.

[42] C. Shukunami, A. Takimoto, M. Oro, Y. Hiraki, Scleraxis positively regulates the expression of tenomodulin, a differentiation marker of tenocytes, Dev Biol 298 (2006) 234–247. https://doi.org/10.1016/j.ydbio.2006.06.036.

[43] J. Hwang, S.Y. Lee, C.H. Jo, Degenerative tendon matrix induces tenogenic differentiation of mesenchymal stem cells, J Exp Orthop 10 (2023). https://doi.org/10.1186/s40634-023-00581-4.

[44] F. Chen, R. Guo, S. Itoh, L. Moreno, E. Rosenthal, T. Zappitelli, R.A. Zirngibl, A. Flenniken, W. Cole, M. Grynpas, L.R. Osborne, W. Vogel, L. Adamson, J. Rossant, J.E. Aubin, First mouse model for combined osteogenesis imperfecta and ehlers-danlos syndrome, Journal of Bone and Mineral Research 29 (2014) 1412–1423. https://doi.org/10.1002/jbmr.2177.

[45] E. Havis, M.-A. Bonnin, I. Olivera-Martinez, N. Nazaret, M. Ruggiu, J. Weibel, C. Durand, M.-J. Guerquin, C. Bonod-Bidaud, F. Ruggiero, R. Schweitzer, D. Duprez, Transcriptomic analysis of mouse limb tendon cells during development, Development (Cambridge) 141 (2014). https://doi.org/10.1242/dev.108654.

[46] V. Bériziat, C. Mazurier, M. Auclair, N. Ferrand, S. Jolly, T. Marie, L. Kobari, I. Toillon, F. Delhommeau, B. Fève, A.K. Larsen, M. Sabbah, L. Garderet, Systemic dysfunction of osteoblast differentiation in adipose-derived stem cells from patients with multiple myeloma, Cells 8 (2019) 1–16. https://doi.org/10.3390/cells8050441.

[47] J. Gorwood, T. Ejlalmanesh, C. Bourgeois, M. Mantecon, C. Rose, M. Atlan, D. Desjardins, R. Le Grand, B. Fève, O. Lambotte, J. Capeau, V. Bériziat, C. Lagathu, SIV Infection and the HIV Proteins Tat and Nef Induce Senescence in Adipose Tissue and Human Adipose Stem Cells, Resulting in Adipocyte Dysfunction, Cells 9 (2020). https://doi.org/10.3390/cells9040854.

[48] Z. Kapacee, S.H. Richardson, Y. Lu, T. Starborg, D.F. Holmes, K. Baar, K.E. Kadler, Tension is required for fibripositor formation, Matrix Biology 27 (2008) 371–375. https://doi.org/10.1016/j.matbio.2007.11.006.

[49] D. Schulz Torres, T.M. Freyman, I. V. Yannas, M. Spector, Tendon cell contraction of collagen-GAG matrices in vitro: Effect of cross-linking, Biomaterials 21 (2000) 1607–1619. https://doi.org/10.1016/S0142-9612(00)00051-X.

[50] M.B. Vaughan, G. Xu, T.L. Morris, P. Kshetri, J.X. Herwig, Predictable fibroblast tension generation by measuring compaction of anchored collagen matrices using microscopy and optical coherence tomography, Cell Adh Migr 13 (2019) 303–314. https://doi.org/10.1080/19336918.2019.1644855.

[51] J. Peltonen, N.J. Cronin, L. Stenroth, T. Finni, J. Avela, Viscoelastic properties of the achilles tendon in vivo, Springerplus 2 (2013) 1–8. https://doi.org/10.1186/2193-1801-2-212.

[52] B.K. Connizzo, A.J. Grodzinsky, Tendon exhibits complex poroelastic behavior at the nanoscale as revealed by high-frequency AFM-based rheology, J Biomech 54 (2017) 11–18. https://doi.org/10.1016/j.jbiomech.2017.01.029.

[53] H. Van Hoorn, N.A. Kurniawan, G.H. Koenderink, D. Iannuzzi, Local dynamic mechanical analysis for heterogeneous soft matter using ferrule-top indentation, Soft Matter 12 (2016) 3066–3073. https://doi.org/10.1039/c6sm00300a.

[54] G. Chen, X. She, Y. Yin, J. Ma, Y. Gao, H. Gao, H. Qin, J. Fang, Targeting TM4SF1 exhibits therapeutic potential via inhibition of cancer stem cells, Signal Transduct Target Ther 7 (2022) 2–5. https://doi.org/10.1038/s41392-022-01177-7.

[55] Z. Yan, X. Cheng, T. Wang, X. Hong, G. Shao, C. Fu, Therapeutic potential for targeting Annexin A1 in fibrotic diseases, Genes Dis 9 (2022) 1493–1505. https://doi.org/10.1016/j.gendis.2022.05.038.

[56] A. Bharadwaj, E. Kempster, D.M. Waisman, The annexin a2/s100a10 complex: The mutualistic symbiosis of two distinct proteins, Biomolecules 11 (2021) 1–18. https://doi.org/10.3390/biom11121849.

[57] Y. Izu, H.L. Ansorge, G. Zhang, L.J. Soslowsky, P. Bonaldo, M.L. Chu, D.E. Birk, Dysfunctional tendon collagen fibrillogenesis in collagen VI null mice, Matrix Biology 30 (2011) 53–61. https://doi.org/10.1016/j.matbio.2010.10.001.

[58] H.L. Ansorge, X. Meng, G. Zhang, G. Veit, M. Sun, J.F. Klement, D.P. Beason, L.J. Soslowsky, M. Koch, D.E. Birk, Type XIV collagen regulates fibrillogenesis: Premature

collagen fibril growth and tissue dysfunction in null mice, Journal of Biological Chemistry 284 (2009) 8427–8438. https://doi.org/10.1074/jbc.M805582200.

[59] O. Okamoto, S. Fujiwara, Dermatopontin, a Novel Player in the Biology of the Extracellular Matrix, Connect Tissue Res 47 (2006) 177–189. https://doi.org/10.1080/03008200600846564.

[60] A.J. de Micheli, J.B. Swanson, N.P. Disser, L.M. Martinez, N.R. Walker, D.J. Oliver, B.D. Cosgrove, C.L. Mendias, Single-cell transcriptomic analysis identifies extensive heterogeneity in the cellular composition of mouse Achilles tendons, Am J Physiol Cell Physiol 319 (2020) C885–C894. https://doi.org/10.1152/ajpcell.00372.2020.

[61] T. Omoto, D. Yimiti, Y. Sanada, M. Toriyama, C. Ding, Y. Hayashi, Y. Ikuta, T. Nakasa, M. Ishikawa, M. Sano, M. Lee, T. Akimoto, C. Shukunami, S. Miyaki, N. Adachi, Tendon-Specific Dicer Deficient Mice Exhibit Hypoplastic Tendon Through the Downregulation of Tendon-Related Genes and MicroRNAs, Front Cell Dev Biol 10 (2022) 1–14. https://doi.org/10.3389/fcell.2022.898428.

[62] G. Zhang, Y. Ezura, I. Chervoneva, P.S. Robinson, D.P. Beason, E.T. Carine, L.J. Soslowsky, R. V. Iozzo, D.E. Birk, Decorin regulates assembly of collagen fibrils and acquisition of biomechanical properties during tendon development, J Cell Biochem 98 (2006) 1436–1449. https://doi.org/10.1002/jcb.20776.

[63] H. Li, A. Korcari, D. Ciufo, C.L. Mendias, S.A. Rodeo, M.R. Buckley, A.E. Loiselle, G.S. Pitt, C. Cao, Increased Ca2+ signaling through CaV 1.2 induces tendon hypertrophy with increased collagen fibrillogenesis and biomechanical properties, FASEB J 37 (2023) e23007. https://doi.org/10.1096/fj.202300607R.

[64] P.P. Purslow, The Structure and Role of Intramuscular Connective Tissue in Muscle Function, Front Physiol 11 (2020). https://doi.org/10.3389/fphys.2020.00495.

[65] J.E. Marturano, J.D. Arena, Z.A. Schiller, I. Georgakoudi, C.K. Kuo, Characterization of mechanical and biochemical properties of developing embryonic tendon, Proceedings of the National Academy of Sciences 110 (2013) 6370 LP – 6375. https://doi.org/10.1073/pnas.1300135110.

[66] N.S. Kalson, D.F. Holmes, Z. Kapacee, I. Otermin, Y. Lu, R.A. Ennos, E.G. Canty-Laird, K.E. Kadler, An experimental model for studying the biomechanics of embryonic tendon: Evidence that the development of mechanical properties depends on the actinomyosin machinery, Matrix Biology 29 (2010) 678–689. https://doi.org/10.1016/j.matbio.2010.08.009.

[67] N.D. Murchison, B.A. Price, D.A. Conner, D.R. Keene, E.N. Olson, C.J. Tabin, R. Schweitzer, Regulation of tendon differentiation by scleraxis distinguishes force-transmitting tendons from muscle-anchoring tendons, Development 134 (2007) 2697 LP – 2708. https://doi.org/10.1242/dev.001933.

[68] C.L. Mendias, J.P. Gumucio, K.I. Bakhurin, E.B. Lynch, S. V. Brooks, Physiological loading of tendons induces scleraxis expression in epitenon fibroblasts, Journal of Orthopaedic Research 30 (2012) 606–612. https://doi.org/10.1002/jor.21550.

[69] F. Fu, X. Yang, M. Zheng, Q. Zhao, K. Zhang, Z. Li, H. Zhang, S. Zhang, Role of Transmembrane 4 L Six Family 1 in the Development and Progression of Cancer, Front Mol Biosci 7 (2020) 1–15. https://doi.org/10.3389/fmolb.2020.00202.

[70] A. Saraswathibhatla, D. Indana, O. Chaudhuri, Cell-extracellular matrix mechanotransduction in 3D HHS Public Access, Nat Rev Mol Cell Biol 24 (2023) 495–516. https://doi.org/10.1038/s415XX-XXX-XXXX-X.

[71] S.H. Taylor, S. Al-Youha, T. van Agtmael, Y. Lu, J. Wong, D.A. McGrouther, K.E. Kadler, Tendon is covered by a basement membrane epithelium that is required for cell retention and the prevention of adhesion formation, PLoS One 6 (2011). https://doi.org/10.1371/journal.pone.0016337.

[72] H.-T. Liao, Osteogenic potential: Comparison between bone marrow and adipose-derived mesenchymal stem cells, World J Stem Cells 6 (2014) 288. https://doi.org/10.4252/wjsc.v6.i3.288.

[73] B. Fang, Y. Liu, D. Zheng, S. Shan, C. Wang, Y. Gao, J. Wang, Y. Xie, Y. Zhang, Q. Li, The effects of mechanical stretch on the biological characteristics of human adipose-derived stem cells, J Cell Mol Med 23 (2019) 4244–4255. https://doi.org/10.1111/jcmm.14314.

[74] A. Scott, P. Danielson, T. Abraham, G. Fong, A. V. Sampaio, T.M. Underhill, Mechanical force modulates scleraxis expression in bioartificial tendons, Journal of Musculoskeletal Neuronal Interactions 11 (2011) 124–132.

[75] M.A. Bonnin, C. Laclef, R. Blaise, S. Eloy-Trinquet, F. Relaix, P. Maire, D. Duprez, Six1 is not involved in limb tendon development, but is expressed in limb connective tissue under Shh regulation, Mech Dev 122 (2005) 573–585. https://doi.org/10.1016/j.mod.2004.11.005.

[76] K.J. Livak, T.D. Schmittgen, Analysis of Relative Gene Expression Data Using Real-Time Quantitative PCR and the 2−ΔΔCT Method, Methods 25 (2001) 402–408. https://doi.org/10.1006/meth.2001.1262.

[77] M. Waldner, W. Zhang, I.B. James, K. Allbright, E. Havis, J.M. Bliley, A. Almadori, R. Schweizer, J.A. Plock, K.M. Washington, V.S. Gorantla, M.G. Solari, K.G. Marra, J.P. Rubin, Characteristics and immunomodulating functions of adipose-derived and bone marrow-derived mesenchymal stem cells across defined human leukocyte antigen barriers, Front Immunol 9 (2018). https://doi.org/10.3389/fimmu.2018.01642.

[78] M. Bléher, B. Meshko, I. Cacciapuoti, R. Gergondey, Y. Kovacs, D. Duprez, A. L'Honoré, E. Havis, Egr1 loss-of-function promotes beige adipocyte differentiation and activation specifically in inguinal subcutaneous white adipose tissue, Sci Rep 10 (2020) 1–15. https://doi.org/10.1038/s41598-020-72698-w.

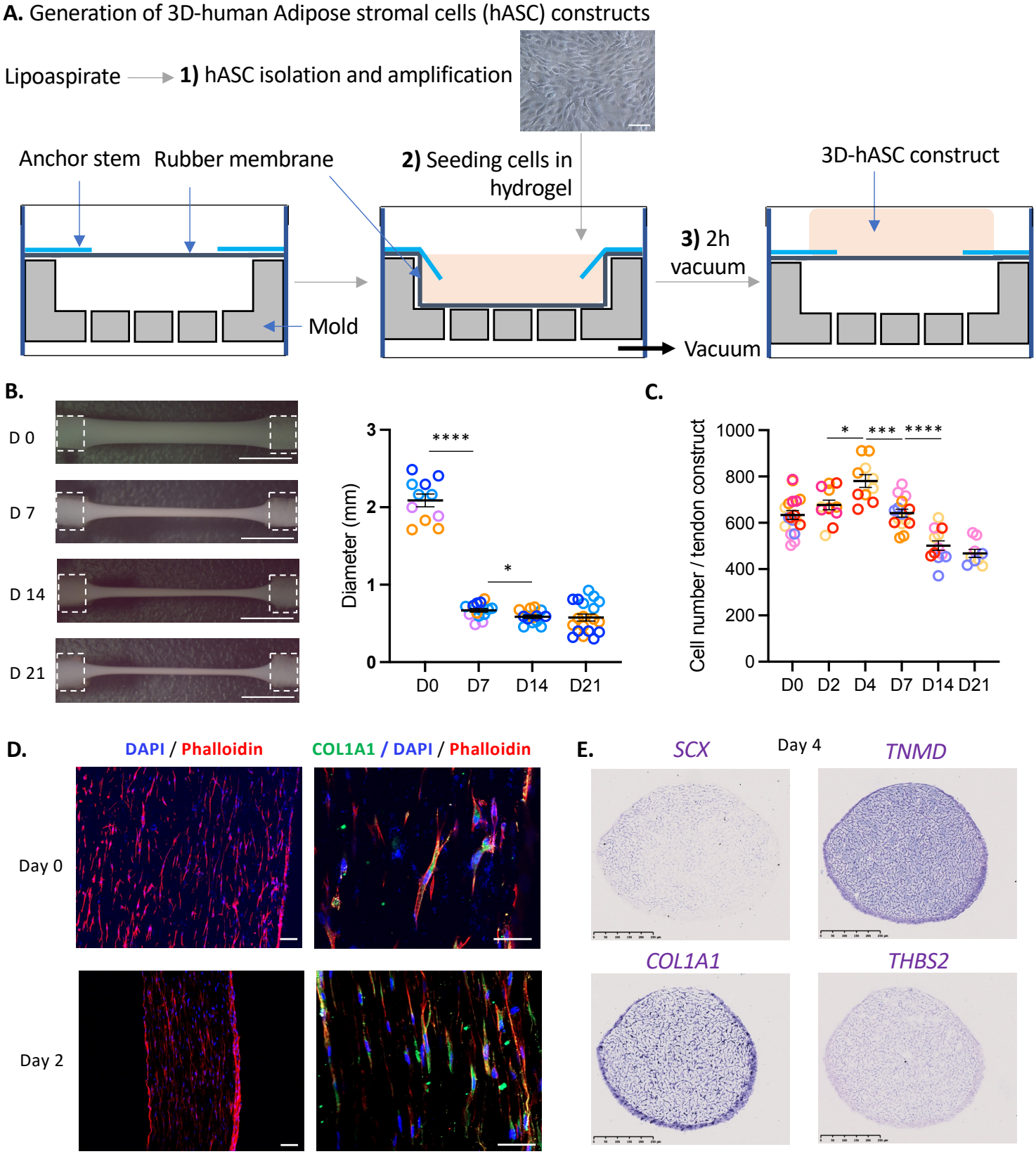
A. Generation of 3D-human Adipose stromal cells (hASC) constructs
Lipoaspirate
1) hASC isolation and amplification
Anchor stem
Rubber membrane
2) Seeding cells in hydrogel
3D-hASC construct
3) 2h vacuum
Mold
Vacuum
B.
D 0
D 7
D 14
D 21
Diameter (mm)
****
*
D0
D7
D14
D21
C.
Cell number / tendon construct
*
***
****
D0
D2
D4
D7
D14
D21
D.
DAPI / Phalloidin
COL1A1 / DAPI / Phalloidin
Day 0
Day 2
E.
SCX
Day 4
TNMD
COL1A1
THBS2

Figure 1

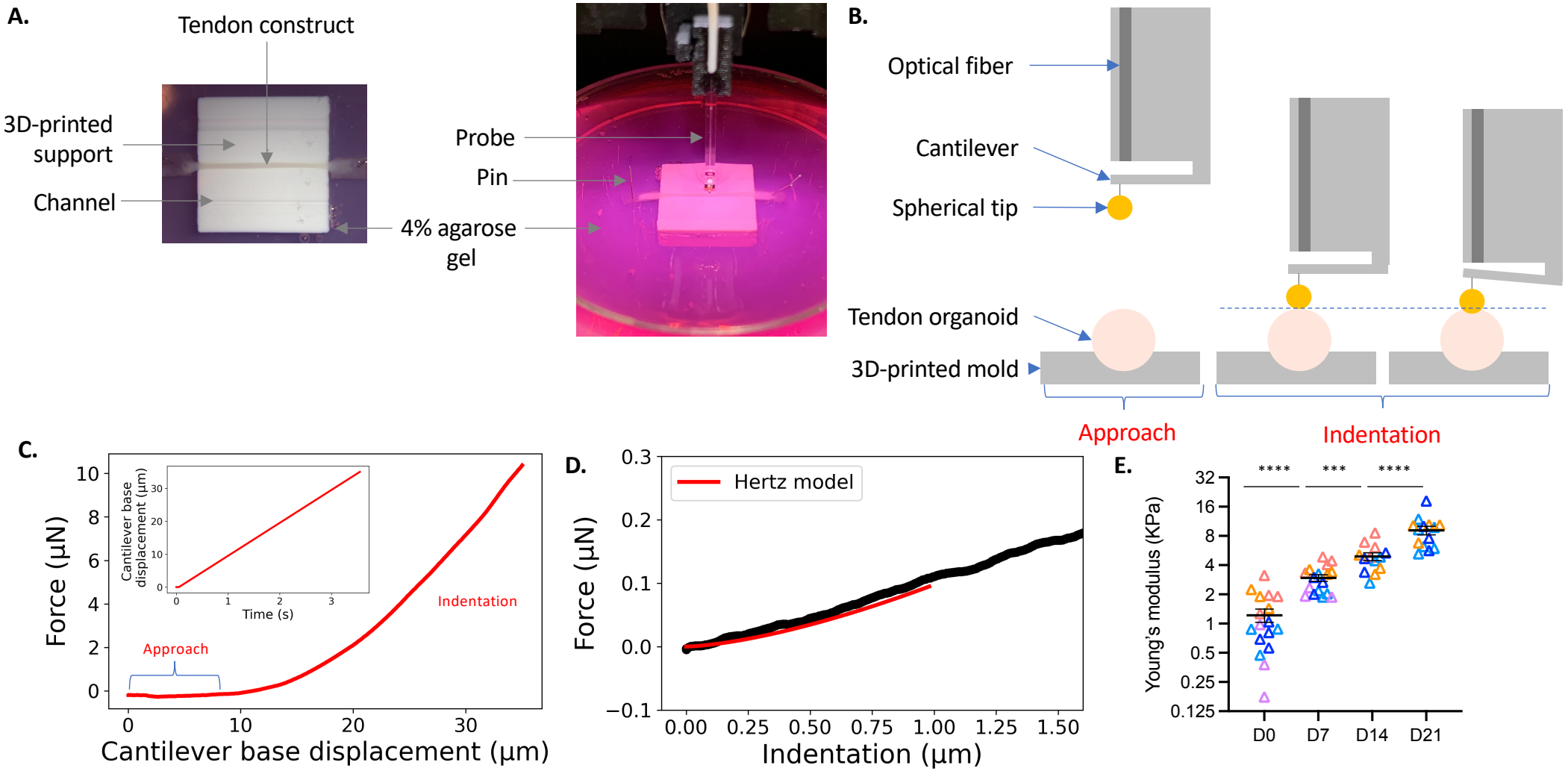
A.
Tendon construct
3D-printed support
Channel
Probe
Pin
4% agarose gel
B.
Optical fiber
Cantilever
Spherical tip
Tendon organoid
3D-printed mold
Approach
Indentation
C.
Force (µN)
Cantilever base displacement (µm)
Cantilever base displacement (µm)
Time (s)
Approach
Indentation
D.
Hertz model
Force (µN)
Indentation (µm)
E.
Young's modulus (KPa)
****
***
****
D0
D7
D14
D21

Figure 2

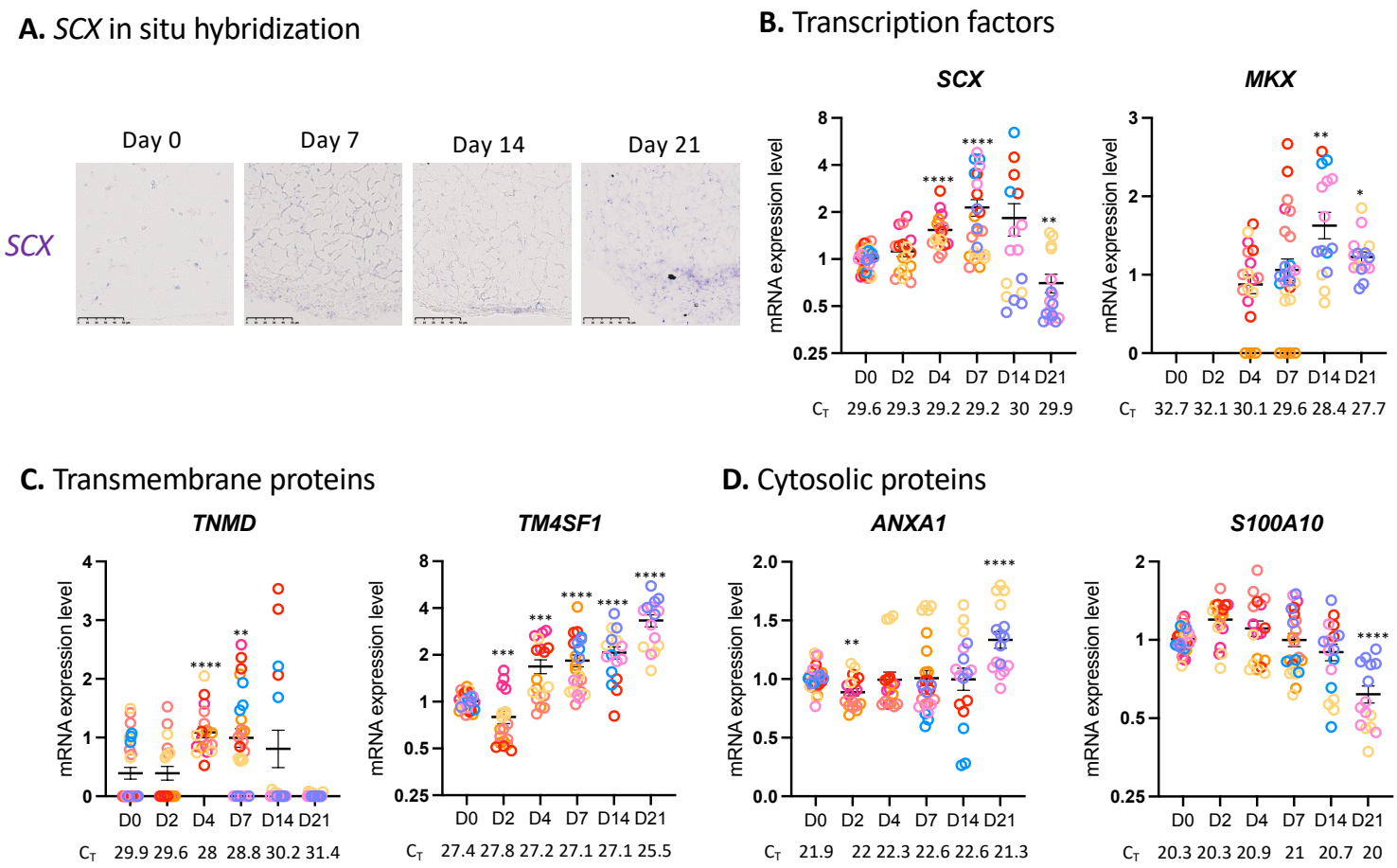
A. SCX in situ hybridization
Day 0
Day 7
Day 14
Day 21
SCX
B. Transcription factors
SCX
MKX
mRNA expression level
D0 D2 D4 D7 D14 D21
C_T 29.6 29.3 29.2 29.2 30 29.9
C_T 32.7 32.1 30.1 29.6 28.4 27.7
C. Transmembrane proteins
TNMD
TM4SF1
C_T 29.9 29.6 28 28.8 30.2 31.4
C_T 27.4 27.8 27.2 27.1 27.1 25.5
D. Cytosolic proteins
ANXA1
S100A10
C_T 21.9 22 22.3 22.6 22.6 21.3
C_T 20.3 20.3 20.9 21 20.7 20

Figure 3

A. *COL1A1* in situ hybridization

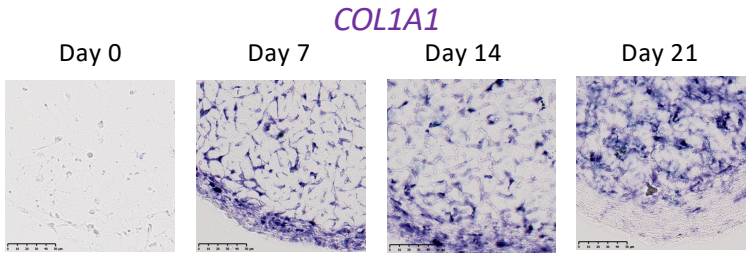

B. Collagens

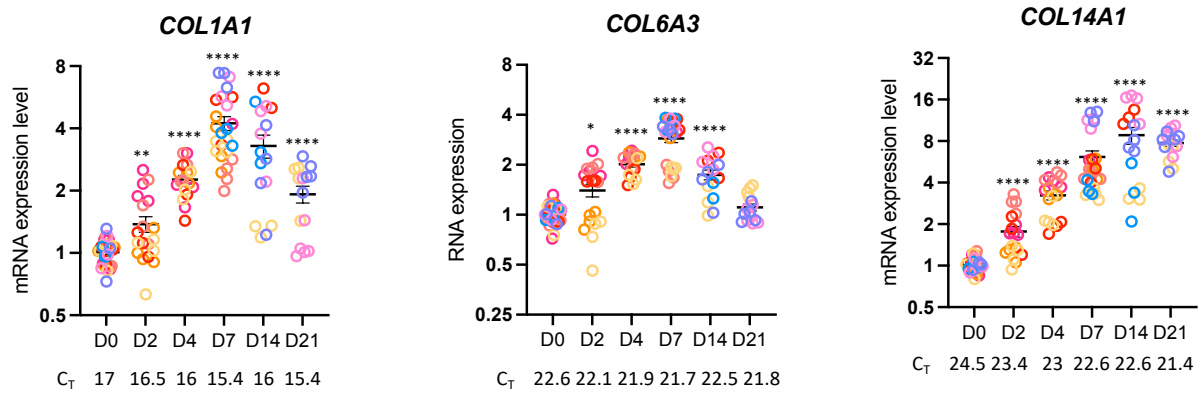

C. Fibrillogenesis

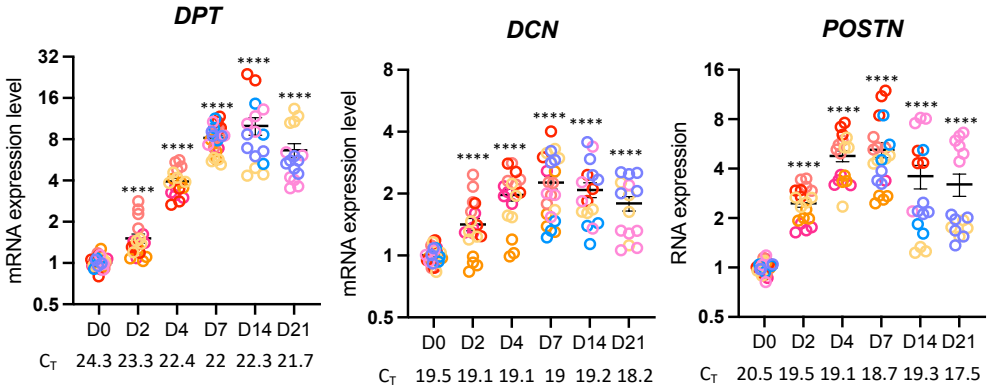

D. *THBS2* (fibrillogenesis) in situ hybridization and RT-qPCR

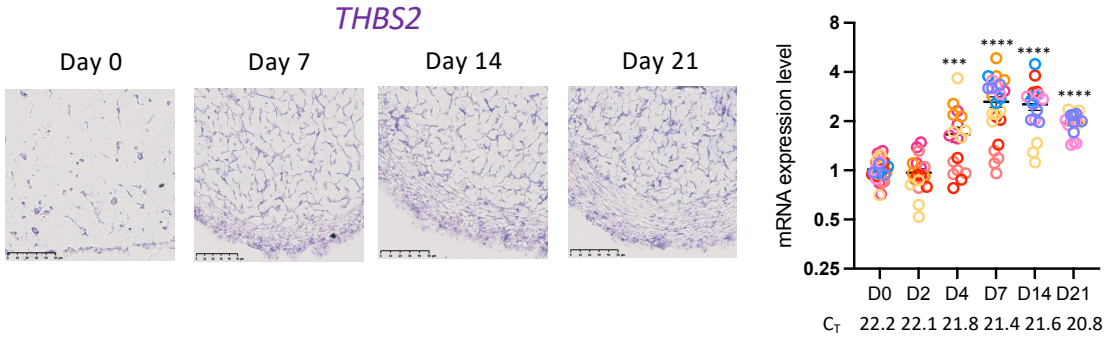

Figure 4

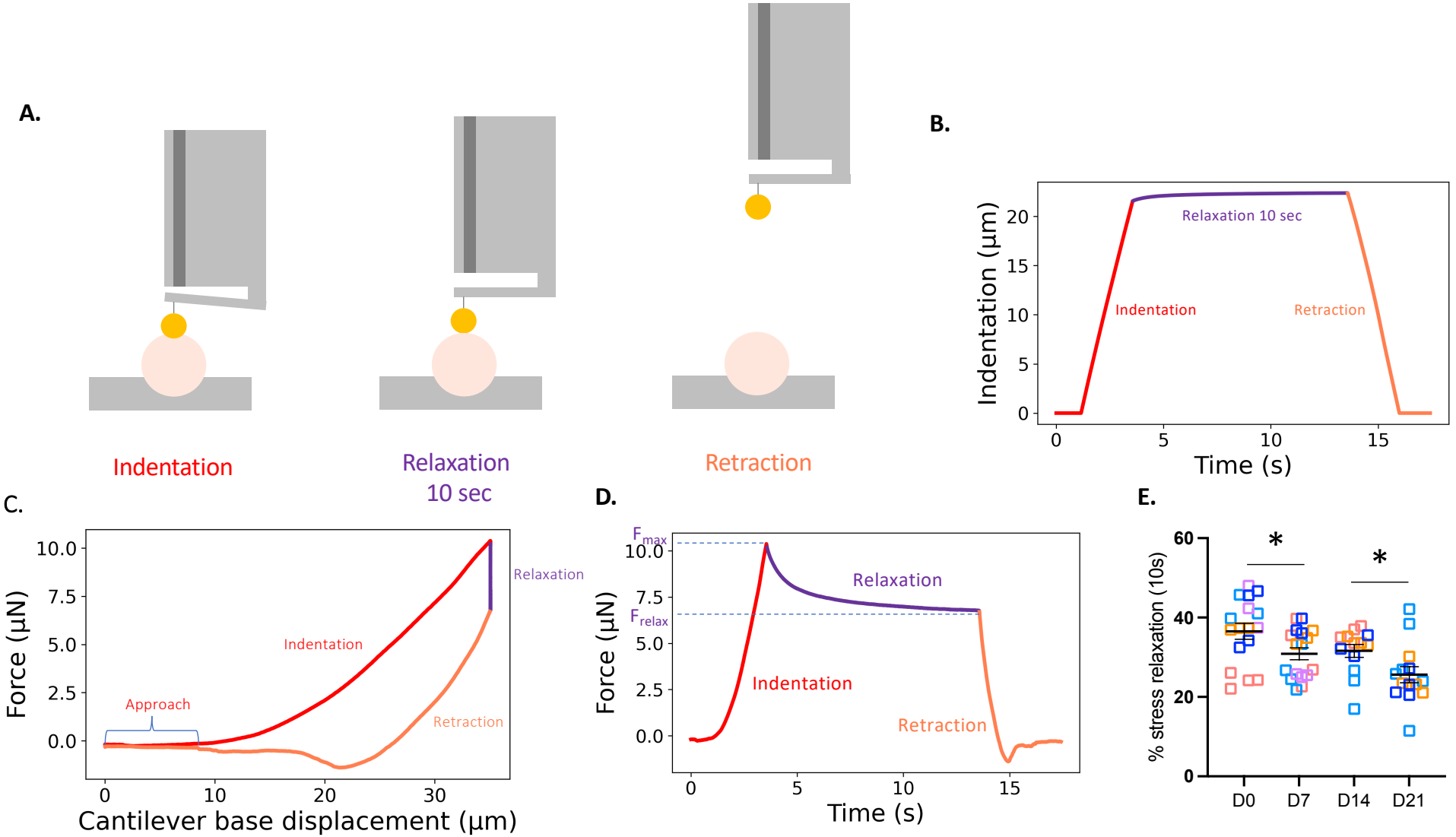
A.
Indentation
Relaxation
10 sec
Retraction
B.
Indentation (µm)
Relaxation 10 sec
Indentation
Retraction
Time (s)
C.
Force (µN)
Relaxation
Indentation
Approach
Retraction
Cantilever base displacement (µm)
D.
F_{max}
F_{relax}
Relaxation
Indentation
Retraction
Force (µN)
Time (s)
E.
% stress relaxation (10s)
D0
D7
D14
D21

Figure 5

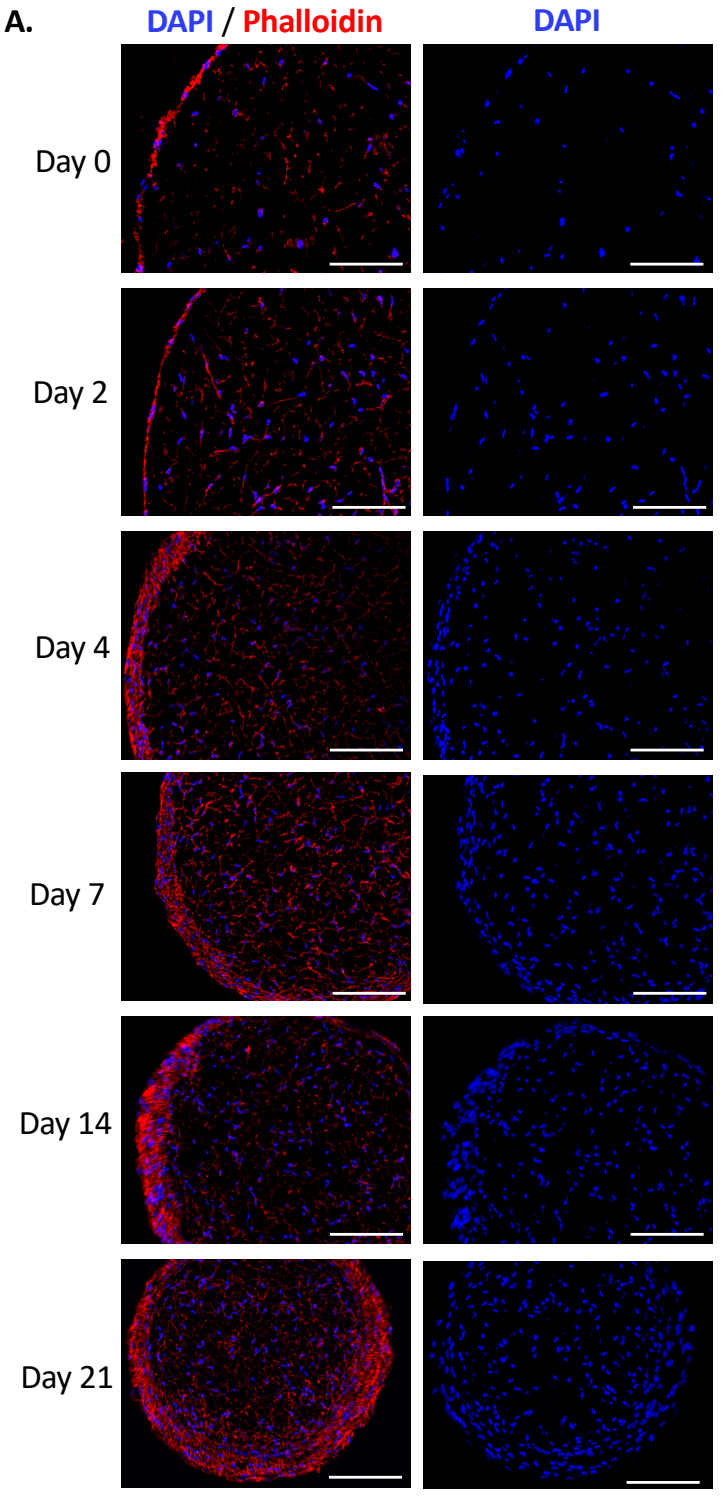
A.
DAPI / Phalloidin
DAPI
Day 0
Day 2
Day 4
Day 7
Day 14
Day 21

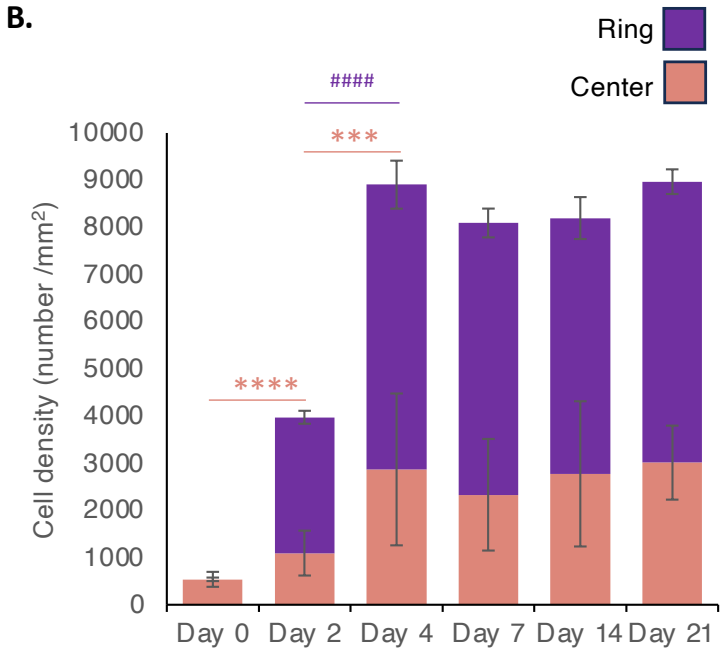
B.
Ring
Center
####
***
****
Cell density (number /mm²)
10000
9000
8000
7000
6000
5000
4000
3000
2000
1000
0
Day 0
Day 2
Day 4
Day 7
Day 14
Day 21

Figure 6